Horizontal Injection of Gas–Liquid Mixtures in a Water Tank

Iran E. Lima Neto[1]; David Z. Zhu, M.ASCE[2]; and Nallamuthu Rajaratnam, F.ASCE[3]

Abstract: Experiments were carried out to investigate the behavior of horizontal gas–liquid injection in a water tank. Measurements of bubble properties and mean liquid flow structure were obtained. The turbulence in the liquid phase appears to help generating bubbles with relatively uniform diameters of 1–4 mm. Both bubble properties and mean liquid flow structure depended on the gas volume fraction and the densimetric Froude number at the nozzle exit. It was found that the bubbles strongly affected the trajectory of the water jet, which behaved similarly to single-phase buoyant jets. However, at gas volume fractions smaller than about 0.15, the water jet completely separated from the bubble core. Bubble slip velocity was also found to be higher than the terminal velocity for isolated bubbles reported in the literature. Dimensionless correlations were proposed to describe bubble characteristics and the trajectory of the bubble plumes and water jets as a function of the gas volume fraction and the densimetric Froude number. Finally, applications of the results for aeration/mixing purposes are presented.

DOI: 10.1061/(ASCE)0733-9429(2008)134:12(1722)

CE Database subject headings: Aeration; Bubbles; Jets; Mixing; Plumes; Gas; Water tanks; Froude number.

Introduction

Air and/or oxygen injection has long been used for artificial aeration and mixing in tanks, lakes, reservoirs, and rivers (see, for example, Whipple and Yu 1970; WPCF 1988; Wüest et al. 1992; Schierholz et al. 2006; Bombardelli et al. 2007). Compared to the injection of single gas phase, the injection of gas–liquid mixtures has additional advantages, such as production of small bubbles without the need for porous diffusers, which are susceptible to clogging, and higher energy efficiency for aeration and mixing purposes (Amberg et al. 1969; Fast and Lorenzen 1976; Sun and Faeth 1986a,b; Iguchi et al. 1997; Mueller et al. 2002). Further, injection of oxygen into an effluent diffuser can also avoid the use of additional air diffusers in river aeration (Lima Neto et al. 2007). In these types of flows, the oxygen transfer rate from the bubbles to the water is usually estimated using the following equation, derived from Fick's law of diffusion (see Mueller et al. 2002):

$$\frac{dC}{dt} = K_L a(C_s - C) \tag{1}$$

where C and C_s=dissolved oxygen (DO) concentration in the water and the saturation concentration, respectively, K_L=liquid film coefficient or mass transfer coefficient; and a=air–water interfacial area per unit liquid volume or specific interfacial area.

In water and wastewater systems such as aeration tanks, ponds, lagoons, and oxidation ditches, where the water depth is usually small compared to the water surface area, the use of horizontal gas–liquid injection is preferable rather than vertical gas–liquid injection in order to increase the contact time between the gas and liquid phases and, as a consequence, to increase the DO concentration in the liquid phase [see Eq. (1)]. In these systems, mixing chambers, Venturi tubes, or ejectors are generally used to mix the gas and the water and discharge the mixture as a series of two-phase buoyant jets that provide both aeration and mixing. These flows are a topic of growing interest because of their high oxygen transfer efficiency and low maintenance and operational costs (Rainer et al. 1995; Morchain et al. 2000; Fonade et al. 2001; Mueller et al. 2002).

There are only limited experimental studies on horizontal gas–liquid injection. Varley (1995) investigated the characteristics of the bubbles where bubble sizes were studied photographically and a correlation based on dimensional analysis for estimating the maximum bubble size was proposed. However, his study was limited to gas-volume fractions at the nozzle, ε, smaller than about 0.23, which is defined as

$$\varepsilon = Q_{a0}/(Q_{a0} + Q_{w0}) \tag{2}$$

where Q_{a0} and Q_{w0}=volumetric flow rates of air and water at the nozzle, respectively. Besides, Varley's measurements were taken only at the nozzle exit and at 10-15 nozzle diameters downstream of the nozzle exit, where bubble breakup and coalescence processes were assumed to be complete. Only bubble size measurements were provided with no other detailed information on bubble characteristics such as bubble velocity and specific interfacial area. On the other hand, Morchain et al. (2000) and Fonade et al. (2001) ignored the buoyancy of the bubbles and estimated the flow circulation patterns induced by horizontal air–water injection in water assuming the same behavior of single-phase horizontal jets.

In this technical paper, we conduct an experimental study to

[1]Ph.D. Candidate, Dept. of Civil and Environmental Engineering, Univ. of Alberta, Edmonton AB, Canada T6G 2W2. E-mail: limaneto@ualberta.ca

[2]Professor, Dept. of Civil and Environmental Engineering, Univ. of Alberta, Edmonton AB, Canada T6G 2W2. E-mail: david.zhu@ualberta.ca

[3]Professor Emeritus, Dept. of Civil and Environmental Engineering, Univ. of Alberta, Edmonton AB, Canada T6G 2W2. E-mail: nrajaratnam@ualberta.ca

Note. Discussion open until May 1, 2009. Separate discussions must be submitted for individual papers. The manuscript for this paper was submitted for review and possible publication on August 22, 2007; approved on June 7, 2008. This paper is part of the ***Journal of Hydraulic Engineering***, Vol. 134, No. 12, December 1, 2008. ©ASCE, ISSN 0733-9429/2008/12-1722–1731/$25.00.

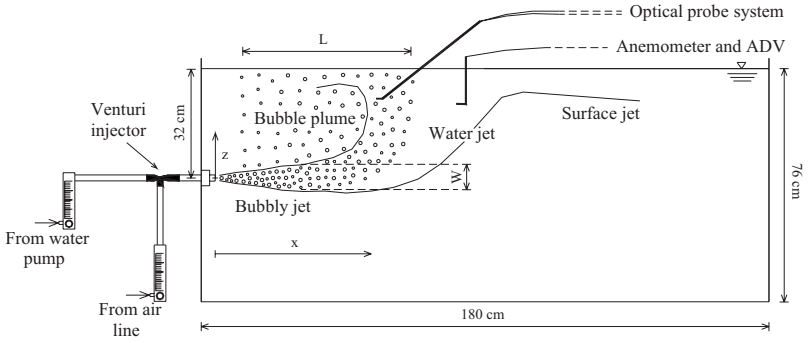

Fig. 1. Schematic of experimental setup

investigate bubble properties and mean liquid flow structure generated due to horizontal air–water injection with gas volume fractions at the nozzle ranging from 0.13 to 0.63. The results obtained here are important for estimating the performance of jet aeration systems and to validate computational fluid dynamics (CFD) codes for simulation of such flows.

Experimental Setup and Procedure

The tests were conducted in a rectangular glass tank with a length of 1.8 m, width of 1.2 m, and height of 0.80 m, shown schematically in Fig. 1. The tank was filled with tap water to a depth of 0.76 m. The gas supply was taken from an air line, whereas the water was pumped from a small reservoir, and both air and water temperatures were fixed at about 20°C. A pressure-regulating valve was used to keep the air pressure at 1 atm (gauge) and ensure a constant flow rate. Volumetric flow rates of air, Q_{a0}, and water, Q_{w0}, were adjusted by rotameters; mixed into a Venturi injector (Model 484, Mazzei Injector Corporation); and then discharged horizontally at the shorter plane of the tank through a single orifice nozzle of 0.6 cm in diameter, d_0. The nozzle was placed at the tank centerline with its exit located at $x=0$ and $z=0$ (see Fig. 1). Table 1 summarizes the experimental conditions.

Typical images of the bubbles for each experimental condition are shown in Fig. 2. A 500 W halogen lamp was used for background illumination, and the images were acquired using a high resolution CCD camera (1,392×1,040 pixels) (TM-1040, Pulnix Inc.) controlled by a computer frame grabber system (Streams 5, IO Industries Inc.) with a frame rate of 30 frames per second (fps)and an exposure time of 1/2,000 s.

Table 1. Summary of Experimental Conditions: Gas Volume Fraction (ε), Reynolds Number (R), and Densimetric Froude Number (F) Are Defined by Eqs. (2), (5), and (7), Respectively

Experiments	Q_{a0} (L/min)	Q_{w0} (L/min)	ε	R	F
1–3	1	3	0.25	10,610	7.3
1–5	1	5	0.17	17,684	12.2
1–7	1	7	0.13	24,757	17.0
3–3	3	3	0.50	10,610	7.3
3–5	3	5	0.38	17,684	12.2
3–7	3	7	0.30	24,757	17.0
5–3	5	3	0.63	10,610	7.3
5–5	5	5	0.50	17,684	12.2
5–7	5	7	0.42	24,757	17.0

Measuring the turbulent liquid flow field within the bubble core using particle image velocimetry was difficult as our flows had relatively high void fractions. As a result, the laser light reflected from the bubbles saturated the camera and corrupted the images of tracer particles. Alternatively, visualization of the entrained liquid jet was achieved using laser-induced fluorescence (LIF). A similar LIF system has been used by Socolofsky and Adams (2002) for visualization of the entrained flow induced by bubble plumes.

Measurements of the mean vertical water velocity along the centerline of the bubble core and the water jet centerline outside the bubble core were performed at a height above the nozzle exit z of 24 cm with an electromagnetic propeller anemometer (Omni Instruments, MiniWater20) with an internal diameter of 22 mm (see Fig. 1). This anemometer is suitable for velocities higher than 2 cm/s, with an accuracy of 2% when used in pure water. Similar propeller anemometers have been used to measure the mean vertical water velocity in bubble plumes and the measurement error due to air bubbles in the water is deemed negligible for local void fractions lower than 2.5% (at $z=24$ cm), as is the case in this study (see Milgram 1983; Riess and Fanneløp 1998). The reliability of our propeller anemometer for measuring vertical bubbly flows with void fractions of up to 3.5% was also confirmed by Lima Neto et al. (2008a). The measurements outside the bubble core were also verified with an acoustic Doppler velocimeter (ADV) (SonTek 1997). This ADV can measure velocities from about 1.0 mm/s to 2.5 m/s at a sampling rate of 25 Hz.

A double-tip optical fiber probe system (RBI Instrumentation) based on the phase-detection technique was used to measure bubble properties. It consists of a module that emits infrared light through two fiber-optic cables to the tips of the probe, 2 mm apart. Each tip extends 1.5 cm and is sharpened into a 30 μm diameter. Emitted light is reflected back to the module when the tips pierce a bubble, resulting in a two-state signal which is recorded at a sampling rate of up to 1 MHz. Absolute bubble velocity is obtained through a cross-correlation analysis of the signals from the two tips of the probe. The same system has been used to measure bubble properties in vertical bubble plumes and bubbly jets (Lima Neto et al. 2008a,c) Similar RBI double-tip optical fiber probe systems have also been used for other bubbly flows (Boes and Hager 2003; Murzyn et al. 2005).

The optical probe signals were processed to calculate the local void fraction (α), bubble frequency (f_b), and absolute bubble velocity (u_b) and the following equations (see Chanson 2002) were used to estimate the specific interfacial area (a) and bubble volume-equivalent sphere diameter (d_b):

$$a = 4f_b/u_b \tag{3}$$

J. Hydraul. Eng., 2008, 134(12): 1722-1731

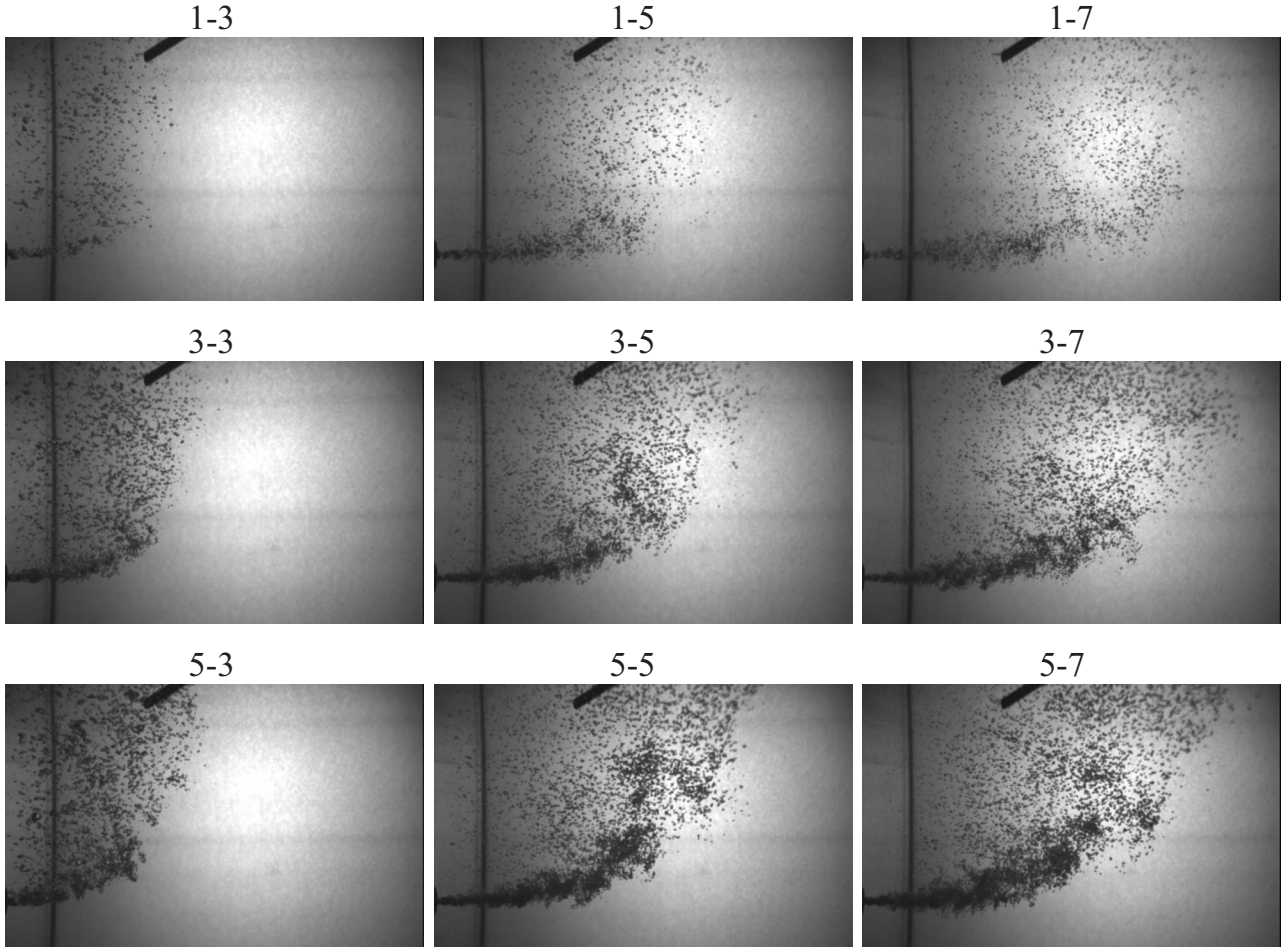

Fig. 2. Typical images (32×50 cm^2) of the bubbles for each experimental condition, showing the tip of the optical probe located at $x = 16$ cm and $z = 24$ cm

$$d_b = 6\alpha/a \tag{4}$$

The optical probe measurements were taken along the bubble core centerline at a height above the nozzle exit z of 24 cm, which was far enough for bubble breakup/coalescence processes to be complete and the bubbles to rise approximately in a rectilinear path.

A carriage mounted on the tank was used for both propeller anemometer and optical probe measurements in order to record data at different longitudinal distances from the nozzle, but the tests were conducted separately for each device. Each test was performed for a duration of 2 min (for each longitudinal distance from the nozzle), which was long enough to obtain stable measurements. The increase in water level due to water injection in the tank was less than 1% over the duration of each test, and this effect was considered negligible. This additional volume of water was then removed from the tank at the end of each test using an overflow pipe.

Experimental Results and Analysis

Bubble Properties

Typical images of the bubbles generated due to horizontal air–water injection in the tank are shown in Fig. 2. Relatively uniform bubbles with diameters ranging from about 1 to 4 mm were observed visually. This is consistent with previous experimental results on vertical air–water bubbly jets (Lima Neto et al. 2008c), where bubbles with approximately uniform sizes were generated when the Reynolds number at the nozzle exit [given by Eq. (5)] exceed a limit of about $\mathrm{R} = 8{,}000$

$$\mathrm{R} = U_{w0} d_0 / \nu_w \tag{5}$$

where ν_w = kinematic viscosity of water and U_{w0} = superficial water velocity given by

$$U_{w0} = Q_{w0}/(\pi d_0^2/4) \tag{6}$$

Approximately uniform bubble diameters, ranging from about 0.3 to 2 mm, were also observed photographically by Varley (1995) in his experiments on disperse horizontal bubbly jets with $\mathrm{R} > 15{,}000$, but the measurements were taken only at the nozzle exit and at 10–15 nozzle diameters downstream of the nozzle exit. Our preliminary tests with $\mathrm{R} < 8{,}000$ confirmed that for this condition the bubbles were much larger and irregular in size and shape, and the bubble core was much shorter. Therefore, the results presented here are limited to experiments with $\mathrm{R} > 8{,}000$, which are expected to be more efficient for aeration purposes. All the following analyses in this technical paper will be based on the densimetric Froude number [given by Eq. (7)], as both momentum and buoyancy forces are expected to affect the behavior of the air-water jets, similarly to single-phase buoyant jets (see Jirka 2004)

J. Hydraul. Eng., 2008, 134(12): 1722-1731

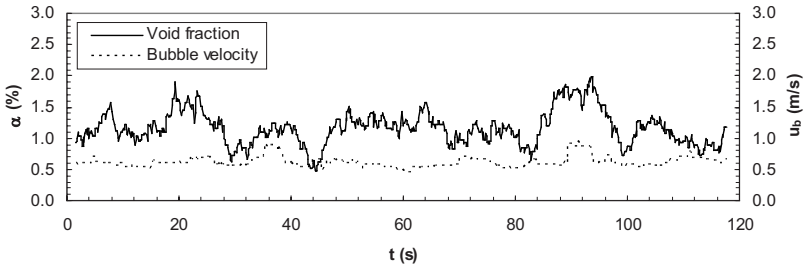

Fig. 3. Typical void fraction and absolute bubble velocity time series. Measurements taken at $x=28$ cm and $z=24$ cm (Experiment 3-5).

$$\mathsf{F} = U_{w0}/\sqrt{g' d_0} \tag{7}$$

where g' = reduced gravity given by

$$g' = g(\rho_w - \rho_a)/\rho_w \tag{8}$$

in which ρ_w and ρ_a = density of water and air, respectively.

As sketched in Fig. 1, two regions are clearly observed in Fig. 2: a quasi-horizontal bubbly jet, where bubble breakup/coalescence processes were observed visually; and a quasi-vertical bubble plume, where the bubbles rose approximately in a rectilinear path with no significant occurrence of breakup/coalescence. Note that part of this bubble plume was formed by some coalesced bubbles that escaped from the quasi-horizontal bubbly jet, especially for the tests with higher values of ε and lower values of F, where bubble coalescence processes appeared to dominate bubble breakup processes. Little lateral spreading of the bubble core from the quasi-horizontal bubbly jet to the quasi-vertical bubble plume was observed visually. Therefore, assuming that the width of the bubble core is equal to the average diameter of the quasi-horizontal bubbly jet (W) and that the length of the bubble core is equal to the length of the bubble plume at $z=24$ cm (L) (see sketch in Fig. 1), we can see from Fig. 2 that the approximate width and length of the bubble core range from about 2 to 5 cm from and 17 to 40 cm, respectively, both increasing with the gas volume fraction and the densimetric Froude number. It can also be observed that the bubbly jet slightly deflects toward the vertical as the gas volume fraction increases.

A low-frequency lateral oscillation of the bubble core was also observed visually in the tests. The occurrence of such oscillations, also called wandering motions, is usually attributed to buoyancy driven instabilities and the effect of the tank walls (see Rensen and Roig 2001; García and García 2006; Lima Neto et al. 2008b). Fig. 3 shows typical void fraction and absolute bubble velocity time series measured with the optical fiber probe system. The average values of α and u_b are 1.2% and 0.6 m/s, respectively. The frequency of oscillation was about 0.05 Hz (more clearly observed from the void fraction time series) and the magnitude of the oscillations was smaller for the velocity time series.

Fig. 4 shows typical bubble size distributions fitted to measurements along the bubble plume centerline with a number of samples ranging from 70 to 900 bubbles for each experimental condition. For all experiments, the distribution resembles lognormal curves with average bubble diameters ranging from 1.8 to 3.4 mm and coinciding approximately with the peaks. Similar distributions were also obtained by Varley (1995). The relatively narrow bands of the distributions confirm that the bubbles generated in our tests were approximately of uniform size, as mentioned earlier (see Fig. 2). It can also be seen that the peaks increase along with the gas volume fraction with the result that more bubbles are generated (e.g., see curves for Experiments 1-3 and 5-3).

Fig. 5 shows the variations along the bubble core centerline of time-averaged void fraction (α); bubble frequency (f_b); absolute bubble velocity (u_b); bubble volume-equivalent sphere diameter (d_b); and interfacial area (a), for each experiment. Figs. 5(a–c) show that α, f, and a follow approximately lognormal distributions. It is clearly seen that the peaks increase as the gas volume fraction increases (e.g., see Experiments 1-5, 3-5, and 5-5), whereas the bubble plumes become longer as the densimetric Froude number increases (e.g., see Experiments 3-3, 3-5, and 3-7). The lengths of the bubble plumes obtained from Fig. 5 ranged from 18 to 44 cm, which are slightly higher than those obtained from the CCD images (see Fig. 2). Figs. 5(c and d) show that u_b and d_b tend to increase as the flow approaches the location of the peak water velocity (see the following section). Note that for the experiments with lower densimetric Froude numbers (i.e., Experiments 1-3, 3-3, and 5-3), larger bubbles escaped from the weaker water jet and the bubble diameter d_b seemed to decrease with the horizontal distance from the nozzle. Moreover, both u_b and d_b appear to increase with the gas volume fraction and decrease with the densimetric Froude number. Similar results were obtained by Varley (1995), who observed an increase in d_b with the air flow rate and a decrease with the water flow rate. Bubble diameters shown in Fig. 5(d) ranged from 1.2 to 3.6 mm and were about 10% smaller than those obtained from the CCD camera images shown in Fig. 2, whereas bubble velocities shown in Fig. 5(c) ranged from 41 to 77 cm/s and were about 25% larger

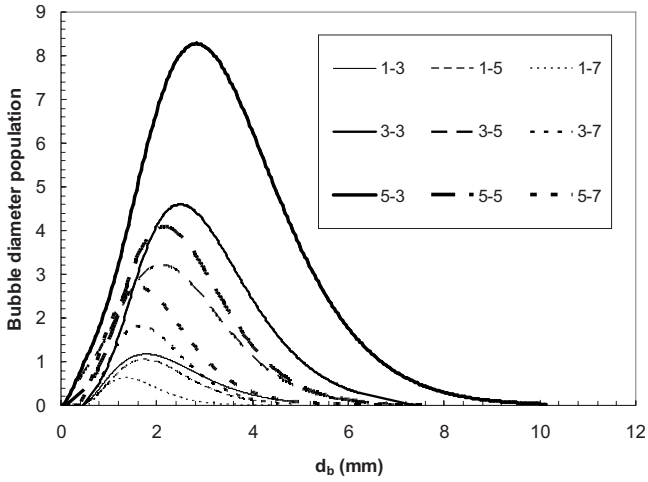

Fig. 4. Typical bubble size distributions obtained by fitting measurements taken at $x=16$ cm and $z=24$ cm

J. Hydraul. Eng., 2008, 134(12): 1722-1731

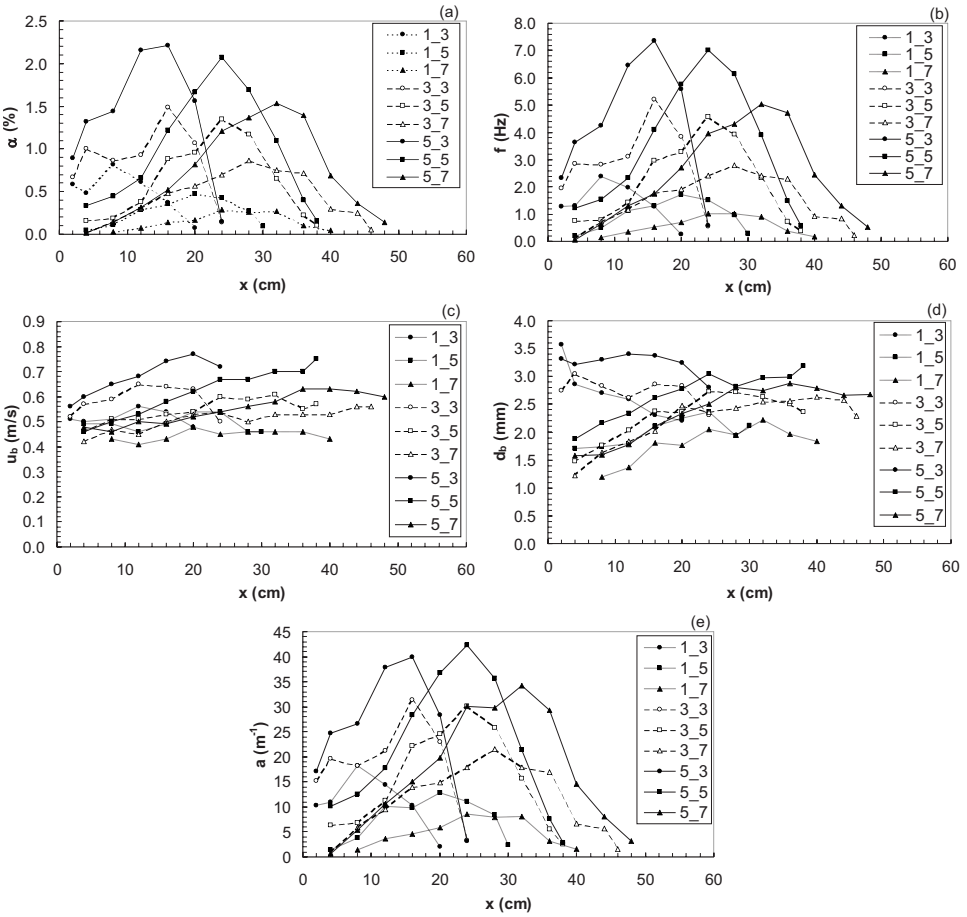

Fig. 5. Variations along the bubble core centerline of: (a) void fraction; (b) bubble frequency; (c) absolute bubble velocity; (d) bubble diameter; and (e) specific interfacial area. Measurements shown were taken at $z=24$ cm.

than those obtained from visual observation. Similar results were obtained with the same techniques in vertical bubble plumes and bubbly jets (Lima Neto et al. 2008a,c).

In order to make the results obtained here applicable to other horizontal gas–liquid injection conditions, dimensional analysis was conducted assuming that the forces due to viscosity, surface tension, and compressibility were negligible compared to the forces due to momentum and buoyancy, under fully turbulent flow conditions in a relatively shallow water tank. The horizontal gas–liquid jet is expected to be controlled by the kinematic fluxes of momentum (controlled by the liquid phase) and buoyancy (controlled by the gas phase), given by $M_0=Q_{w0}U_{w0}$ and $B_0=Q_{a0}g'$, respectively. Thus the length and velocity scales, L_e and U_e, can be defined as $L_e=M_0^{3/4}/B_0^{1/2}$ and $U_e=B_0^{1/2}/M_0^{1/4}$, or

$$L_e=\lfloor(\pi/4)^{1/4}\mathsf{F}d_0\rfloor(Q_{w0}/Q_{a0})^{1/2}=\lfloor(\pi/4)^{1/4}\mathsf{F}d_0\rfloor[(1-\varepsilon)/\varepsilon]^{1/2} \tag{9}$$

$$U_e=\lfloor(\pi/4)^{1/4}\sqrt{g'd_0}\rfloor(Q_{a0}/Q_{w0})^{1/2}=\lfloor(\pi/4)^{1/4}\sqrt{g'd_0}\rfloor[\varepsilon/(1-\varepsilon)]^{1/2} \tag{10}$$

Notice that the above-presented equations are extensions of those for single-phase buoyant jets. For example, for single-phase water jets where the buoyancy is created by temperature or salinity difference, $B_0=Q_{a0}g'=Q_{w0}g'$, and Q_{w0}/Q_{a0} in Eq. (9) simply becomes unity. In single-phase flows, L_e is a useful length scale indicating where the buoyant jet changes from momentum dominated to buoyancy dominated (see Jirka 2004). In bubbly jet flows, L_e is also expected to be a length scale where the bubbles separate from the water jet.

Using the above-presented scales, the following relationships can be obtained:

$$\left[\frac{L}{L_e},\frac{W}{L_e},\frac{u_b}{U_e},\frac{d_b}{L_e},\frac{(K_La)L_e}{U_e}\right]=f(\varepsilon,\mathsf{F}) \tag{11}$$

Thus, measured values of the width (W) and length (L) of the bubble core as well as longitudinal-averaged values of u_b, d_b, and K_La are nondimensionalized and curve fitting of experimental data provided the following correlations:

$$\frac{L}{L_e}=13.491(\varepsilon^{1.1}\mathsf{F}^{-0.1})+0.168 \tag{12}$$

$$\frac{W}{L_e}=1.109(\varepsilon^{1.4}\mathsf{F}^{0.1})+0.026 \tag{13}$$

$$\frac{u_b}{U_e}=1.598\ln(\varepsilon^{-1.2}\mathsf{F}^{-0.1})+1.647 \tag{14}$$

$$\frac{d_b}{L_e}=2.103(\varepsilon^{1.1}\mathsf{F}^{-1.3})+0.001 \tag{15}$$

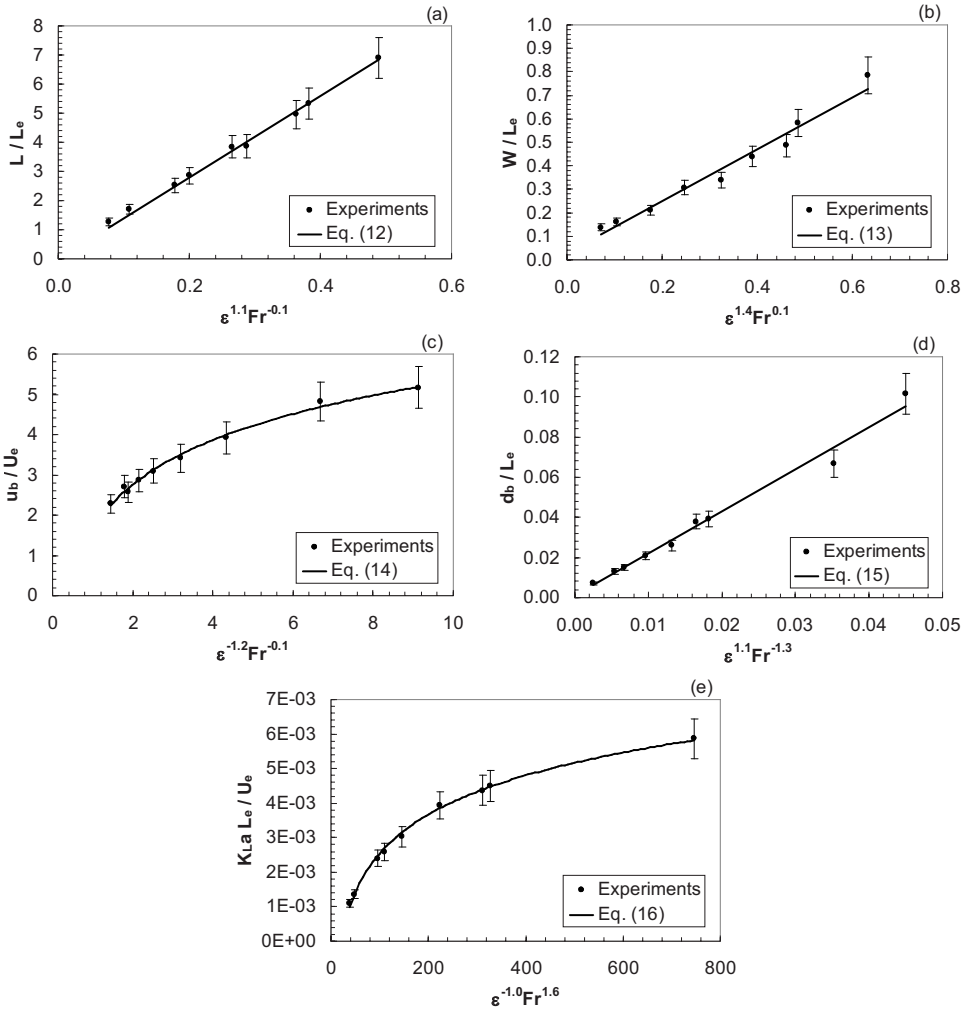

Fig. 6. Adjustment of the dimensionless correlations for (a) length of the bubble core; (b) width of the bubble core; (c) absolute bubble velocity; (d) bubble diameter; and (e) volumetric mass transfer coefficient to experimental data. The error bars indicate deviations of 10% from the mean values, which were estimated from sample tests of reproducibility of the results.

$$\frac{(K_L a)L_e}{U_e} = [1.632 \times \ln(\varepsilon^{-1.0}\mathsf{F}^{1.6}) - 4.977] \times 10^{-3} \qquad (16)$$

In the above-presented correlations, we used a constant mass transfer coefficient $K_L = 4 \times 10^{-4}$ m/s obtained for the range of bubble diameters studied here (see Wüest et al. 1992; McGinnis and Little 2002), which resulted in volumetric mass transfer coefficients $K_L a$ ranging from about 7 to 37 h^{-1}. Note that these correlations are valid for a specific height $z = 24$ cm above the nozzle exit.

Other length and velocity scales have also been used in dealing with gas–liquid two-phase flows. For example, Bombardelli et al. (2007) defined a length scale $D = B_0/4\pi\alpha_e^2 u_s^3$, where α_e = entrainment coefficient and u_s = bubble slip (or relative) velocity. As both momentum and buoyancy at the nozzle are expected to be important in air–water jets, it is logical to define the length scale L_e and the velocity scale U_e as in Eqs. (9) and (10). These scales can be directly calculated from the flow conditions at the nozzle.

Fig. 6 shows that Eqs. (12)–(16) adjusted well to the experimental data, with coefficients of determination ranging from 0.971 to 0.997. This suggests that the parameters adopted here are appropriate to describe the dynamics of the bubbles generated from horizontal gas–liquid injection. Note that we also tested different length scales such as the above-mentioned D and a parameter given by $L_e^* = (Q_{w0}^2/g)^{1/5}$, as well as different velocity scales defined as $U_D = Q_{w0}/D^2$ and $U_e^* = Q_{w0}/(L_e^*)^2$, but the resulting correlation equations did not adjust that well to the experimental data.

The length scale L_e is proportional to d_0 whereas the velocity scale U_e is proportional to $\sqrt{d_o}$ for the same values of ε and F. Hence, if we had for instance a nozzle diameter 2.5 times larger and flow rates 10 times higher than those used in this study (keeping ε and F constant), we would expect bubbles with a diameter and velocity of, respectively, 2.5 and 1.6 times larger. Nevertheless, caution should be taken when using Eqs. (12)–(16) for scaling up of jet aerator systems with much larger nozzle diameters, as the bubble diameter in similar flows (i.e., vertical bubble plumes) is expected to be up to about 40 mm [see the summary in Bombardelli et al. (2007)].

Liquid Flow Structure

Fig. 7 shows a typical sequence of LIF images of the water jet. As sketched in Fig. 1, this water jet follows approximately the trajectory of the bubbles in the bubbly jet region (as momentum dominates buoyancy forces), partially separates from the bubble

J. Hydraul. Eng., 2008, 134(12): 1722-1731

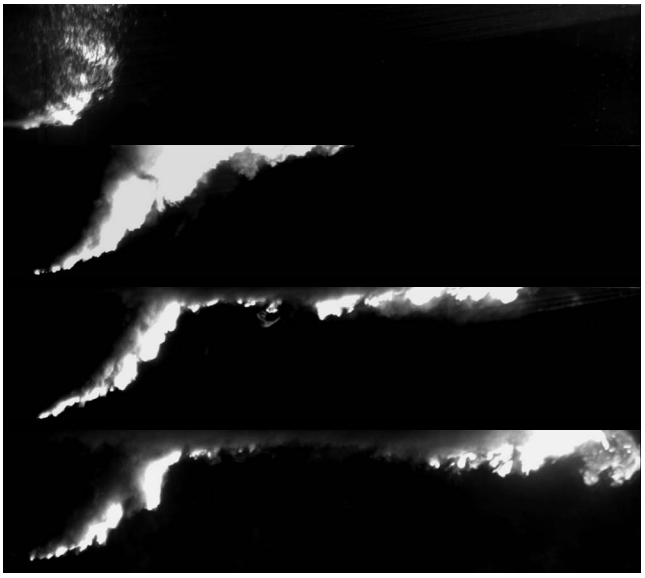

Fig. 7. Typical sequence of LIF images (32×140 cm^2) at times $t=0.0$, 6.7, 13.3, and 20.0 s after dye injection (Experiment 3-5). Note that the bubbles are shown in the first image and the water jet development is shown in the subsequent images. Part of the water jet inside the bubble core cannot be visualized because the bubbles blocked the laser sheet.

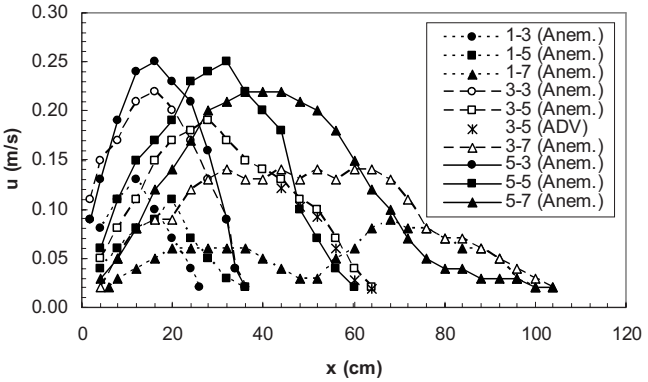

Fig. 8. Typical variations of mean vertical water velocity along the bubble plume/water jet centerline. Measurements shown were taken at $z=24$ cm.

core after some distance from the nozzle (as the bubbles tend to move upwards due to buoyancy forces), and then becomes a surface water jet. This behavior is similar to that of single-phase buoyant jets described by Jirka (2004), except for the separation phenomenon, which has also been observed in bubble plumes in crossflows (see Socolofsky and Adams 2002). The LIF images also showed that recirculation currents formed about 1 min after the beginning of the tests, and oscillations in their position during the experiments probably contributed to the above-mentioned wandering motion of the bubble core, as observed by Lima Neto et al. (2008b) in vertical bubble plumes.

Calculating the horizontal water velocity at the surface jet region from the LIF images, we can estimate the volumetric mass transfer coefficient due to surface aeration at the air–water interface using predictive equations given by Lima Neto et al. (2007). For example, considering a horizontal water velocity of about 5 cm/s (see Fig. 7) and the water depth of 76 cm, we estimated a volumetric mass transfer coefficient of the order of 0.05 h^{-1} for Experiment 3-5, which is much smaller than the corresponding $K_L a$ value of 22 h^{-1} estimated earlier for mass transfer from the bubbles to the water. This implies that most of the oxygen transferred to the water is due to bubble dissolution, even though the contact area between the bubbles and the water is about 20 times smaller than that between the atmosphere and the water.

Part of the water jet inside the bubble core could not be visualized from LIF images because the bubbles blocked the laser sheet. However, propeller anemometer measurements of vertical water velocity, (u), shown in Fig. 8, confirmed that significant velocities were present inside the bubble core, with the velocity distributions roughly resembling lognormal curves. This occurred because of additional entrainment into the wakes of the bubbles, as observed by Leitch and Baines (1989) and Lima Neto et al. (2008c) in experiments with vertical bubble plumes and bubbly jets, respectively. Fig. 8 also shows that the magnitude of the velocities and the penetration lengths increase along with the gas volume fraction (see Experiments 1-5, 3-5 and 5-5), whereas increases in the densimetric Froude number increase the penetration lengths but decrease the peak velocities (see Experiments 3-3, 3-5, and 3-7). It is important to mention that a distinct behavior was observed for Experiment 1-7, where the water jet completely separated from the bubble core at about $x=40$ cm and two peaks are present in the vertical water velocity profiles shown in Fig. 8: one at about $x=30$ cm due to the flow induced by the bubble plume and another at about $x=65$ cm due to the water jet itself. This separation was mainly attributed to the relatively small buoyancy as compared to the high momentum of the water jet (see Table 1). We can thus conclude that a transition gas volume fraction lies between the values of 0.17 and 0.13, which correspond to Experiments 1-5 and 1-7, respectively. We propose that a value of ε smaller than about 0.15 is needed to cause complete separation between the bubble core and water jet.

Trajectory of the Bubble Plumes and Water Jets

Following the procedure described earlier to obtain Eq. (11), dimensional analysis gives these relationships to describe, respectively, the trajectory of the bubble plumes and water jets

$$\left(\frac{z_b}{L_e}\right) = f\left(\varepsilon, \mathsf{F}, \frac{x_b}{L_e}\right) \tag{17}$$

$$\left(\frac{z_w}{L_e}\right) = f\left(\varepsilon, \mathsf{F}, \frac{x_w}{L_e}\right) \tag{18}$$

Hence, assuming that the center of the bubble plumes coincides with the location of the peak void fraction measurements [see Fig. 5(a)], we can normalize our data and obtain the following correlation to describe the trajectory of the bubble plumes:

$$\frac{z_b}{L_e} = \varepsilon^{-1.7}\mathsf{F}^{-1.0}\left[0.983\left(\frac{x_b}{L_e}\right)^2 - 0.069\left(\frac{x_b}{L_e}\right)\right] \tag{19}$$

Fig. 9(a) shows that Eq. (19) fits well to the experimental data, with a coefficient of determination of 0.987. Similarly, assuming that the center of the water jets coincides with the location of the peak vertical water velocities (see Experiment 3-5 in Figs. 7 and 8), we obtain the following correlation to describe the trajectory of the water jets:

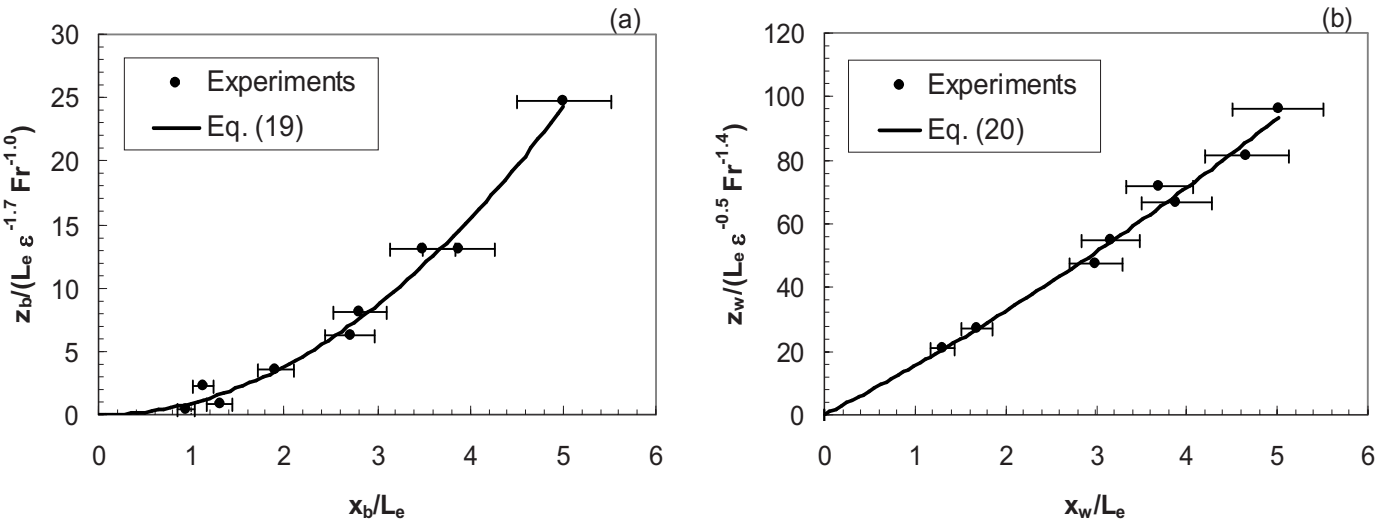

Fig. 9. (a) Dimensionless trajectory of the bubble plumes; (b) dimensionless trajectory of the water jets. Note that data corresponding to Experiment 1-7 (with $\varepsilon < 0.15$) are excluded from the dimensionless trajectory of the water jets because of the occurrence of complete separation from the bubble plume. The error bars indicate deviations of 10% from the mean values, which were estimated from sample tests of reproducibility of the results.

$$\frac{z_w}{L_e} = \varepsilon^{-0.5}\mathsf{F}^{-1.4}\left[0.797\left(\frac{x_w}{L_e}\right)^2 + 14.673\left(\frac{x_w}{L_e}\right)\right] \qquad (20)$$

Fig. 9(b) shows that Eq. (20) also fits well to the experimental data, with a coefficient of determination of 0.988. Note that experimental data corresponding to Experiment 1-7 ($\varepsilon < 0.15$) was excluded from this figure because, in this case, the water jet separated completely from the bubble core, as mentioned earlier. Eq. (20) is important because models for simulation of the flow induced by jet aerator systems usually assume that the behavior of the horizontal water jet is not affected by the bubbles (see Morchain et al. 2000; Fonade et al. 2001).

Bubble Slip Velocity and Shape

With the measurements of vertical water velocity and absolute bubble velocity, we can now estimate the bubble slip velocity, u_s. Fig. 10 shows that bubble slip velocities obtained in this study ranged from about 0.3 to 0.5 m/s and collapsed well within the curve proposed by Lima Neto et al. (2008c) to describe the variation of u_s with d_b in vertical bubbly flows. The above-mentioned values are higher than the terminal bubble velocity of about 0.2 m/s given by Clift et al. (1978) for isolated bubbles of similar diameters. This occurred because trailing bubbles in the wake of leading bubbles rise faster than isolated bubbles due to drag reduction, as observed by Ruzicka (2000) on experiments on bubbles rising in line. The results shown in Fig. 10 are important because models for simulation of bubbly flows usually assume constant slip velocities equal to the terminal bubble velocities given by Clift et al. (1978).

Using the values of u_s and d_b estimated earlier, we can calculate the bubble Reynolds number ($\mathsf{R}_b = u_s d_b/\nu_w$), Eötvös number ($\mathsf{E}_b = g\Delta\rho d_b^2/\sigma$), and Morton number ($\mathsf{M}_b = g\Delta\rho\mu_w^4/\rho_w^2\sigma^3$), where $\Delta\rho$ = difference between the water and air densities; σ = air–water surface tension; and μ_w = viscosity of water. These dimensionless numbers are generally used to express the importance of inertia, buoyancy, surface tension, and viscosity on single bubbles rising in liquids. For the present study, the ranges of R_b and E_b were 480–1755 and 0.2–1.7, respectively, and $\mathsf{M}_b = 3.1 \times 10^{-11}$. According to the classical diagram describing the behavior of isolated bubbles provided by Clift et al. (1978), our values of R_b, E_b and M_b fall within the region of spherical, ellipsoidal, and wobbling regimes, which is in agreement with the shapes observed from the CCD images (see Fig. 2). This trend suggests that the bubbles studied here behaved similarly to isolated bubbles, although their slip velocities were higher. Similar results were obtained by Lima Neto et al. (2008c) for vertical bubbly jets.

Applications

The correlations obtained here can be used for the scaling up of jet aerator systems, as mentioned earlier, as well as to compare the aeration potential of different horizontal air–water injection

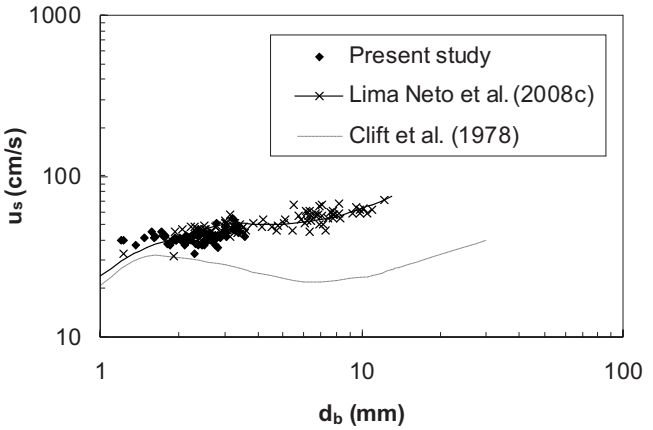

Fig. 10. Bubble slip velocity versus bubble diameter. Dashed and solid lines indicate fitted curves obtained from the literature pertaining to isolated bubbles and vertical bubbly flows, respectively.

J. Hydraul. Eng., 2008, 134(12): 1722-1731

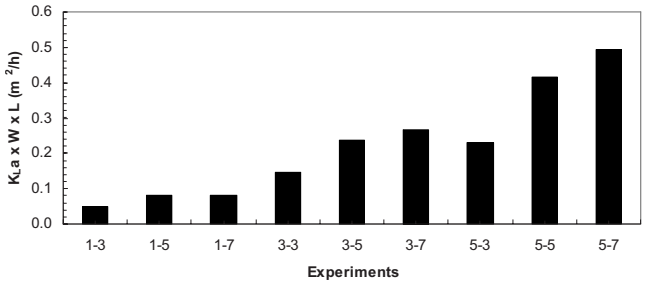

Fig. 11. Estimated aeration potential for each experimental condition

conditions. Defining this aeration potential as the product of the volumetric mass transfer coefficient ($K_L a$) by the approximate area of the bubble core in contact with the water column above the nozzle ($W \times L$), we can estimate, for example, which flow condition studied here is the best for aeration. Fig. 11 shows that, as expected, the experiment with the highest air and water flow rates (Experiment 5-7) corresponds to the best condition for aeration. On the other hand, experiments with relatively high air flow rates and low water flow rates (e.g., Experiment 5-3) may have comparable aeration potential to those with relatively low air flow rates and high water flow rates (e.g., Experiment 3-5), which in turn will result in higher electricity costs for pumping a higher water flow rate. However, in this case, the benefit will be a higher penetration length of the water jet for circulation and mixing as compared to the experiments with lower water flow rates (see Fig. 8). It is important to stress that all experiments conducted here were performed for $\mathrm{R} > 8{,}000$, where bubbles of approximately uniform sizes were generated. For lower values of R, we expect the formation of larger bubbles and reduced aeration potential, as mentioned earlier. Therefore, we recommend that the condition of $\mathrm{R} < 8{,}000$ should be avoided.

Overall, the above-presented results of bubble properties and mean liquid flow structure can also be used to evaluate and validate CFD models for horizontal gas–liquid injection systems. However, caution should be taken when applying these results to systems with different temperatures and high concentration of impurities, which could impact on the two-phase flow behavior and mass transfer characteristics (see Clift et al. 1978; Mueller et al. 2002).

Summary and Conclusions

An experimental study was performed to investigate the behavior of horizontal injection of air–water mixture in a water tank. The experimental conditions included gas volume fractions ranging from 0.13 to 0.63, Reynolds numbers ranging from 10,600 to 24,800, and densimetric Froude numbers ranging from 7 to 17, which produced bubbles of approximately uniform size with volume-equivalent sphere diameters ranging from about 1 to 4 mm.

Two important regions were observed from the images of the bubbles: a quasi-horizontal bubbly jet and a quasi-vertical bubble plume. Bubble size distributions obtained by fitting measurements at the bubble plume region resembled lognormal curves with relatively narrow bands. This confirmed that the bubbles generated in our tests were approximately of uniform size. Time-averaged distributions of bubble properties along the bubble core centerline were found to depend on the gas volume fraction and the densimetric Froude number. The distributions of void fraction, bubble frequency, and interfacial area followed approximately lognormal distributions. On the other hand, absolute bubble velocity and bubble diameter tended to increase with the horizontal distance from the nozzle exit, except for the experiments with higher gas volume fractions and lower densimetric Froude numbers, where larger bubbles escaped from the weaker water jet closer to the nozzle exit. Dimensionless correlations for bubble properties and the trajectory of the bubble plumes as a function of the gas volume fraction and the densimetric Froude number were also obtained by curve fitting of experimental data.

It was found that the water jet followed approximately the trajectory of the bubbles in the bubbly jet region, partially separated from the bubble core after some distance from the nozzle, and then became a surface water jet. Both the peak vertical water velocities and the trajectory of the water jets were found to depend on the gas volume fraction and the densimetric Froude number. However, it was found that the water jet completely separated from the bubble core at gas volume fractions smaller than about 0.15. Excluding such particular conditions, a dimensionless correlation for the water jet trajectory as a function of the gas volume fraction and the densimetric Froude number was also obtained by curve fitting of experimental data. This correlation is important because current models for simulation of the flow generated by horizontal gas–liquid injection usually assume that the trajectory of the water jet is not affected by the presence of the bubbles.

In the above-mentioned correlations, the parameters were normalized by appropriate length and velocity scales defined as functions of the kinematic fluxes of momentum and buoyancy, similarly to those used for single-phase buoyant jets. Provided the gas volume fraction and densimetric Froude number follow the principle of similitude, these correlations are expected to be consistent for purposes of scaling up jet aerator systems. However, as the length scale used in these correlations is proportional to the nozzle diameter and we expect that there is a limit for the maximum bubble size in field-scale bubble plumes, caution should be taken when scaling up jet aerator systems with much larger nozzle diameters.

Bubble slip velocities were found to be higher than the terminal velocities for isolated bubbles reported in the literature, even though their shapes were similar for the same values of Reynolds, Eötvös, and Morton numbers. This was attributed to the fact that trailing bubbles in the wake of leading bubbles rise faster than isolated bubbles due to drag reduction, as reported in the literature pertaining to bubbles rising in line. Bubble slip velocities obtained here could be described as a function of bubble diameter and adjusted well to the curve proposed by Lima Neto et al. (2008c) for vertical bubble plumes and bubbly jets. These results are important because two-phase models for vertical bubbly flows typically assume bubble slip velocities of the same order as those for isolated bubbles.

Finally, applications of the results for estimation of the aeration/mixing potential of different horizontal air–water injection conditions are presented and discussed.

Acknowledgments

The first writer is supported by the Coordination for the Improvement of Higher Education Personnel Foundation (CAPES), Ministry of Education, Brazil. The writers would like to thank Perry Fedun and Chris Krath for building the experimental apparatus.

Notation

The following symbols are used in this paper:

a = air–water specific interfacial area (m^{-1});
B_0 = kinematic flux of buoyancy defined by $B_0=Q_{a0}g'$ (m^4/s^3);
C = dissolved oxygen (DO) concentration in water (mg/L);
C_s = saturation DO concentration in water (mg/L);
d_b = bubble volume-equivalent sphere diameter (mm);
d_0 = nozzle diameter (cm);
F = densimetric Froude number defined by Eq. (7);
f = bubble frequency (Hz);
g' = reduced gravity defined by Eq. (8) (m/s^2);
K_L = mass transfer coefficient (m/s);
L = length of the bubble core defined in Fig. 1 (cm);
L_e = length scale defined by $L_e=M_0^{3/4}/B_0^{1/2}$ or Eq. (9) (cm);
M_0 = kinematic flux of momentum defined by $M_0=Q_{w0}U_{w0}$ (m^4/s^2);
Q_{a0} = air flow rate at the nozzle (L/min);
Q_{w0} = water flow rate at the nozzle (L/min);
R = Reynolds number defined by Eq. (5);
U_e = velocity scale defined by $U_e=B_0^{1/2}/M_0^{1/4}$ or Eq. (10) (cm/s);
U_{w0} = superficial water velocity at the nozzle exit (cm/s);
u = vertical water velocity (m/s);
u_b = absolute bubble velocity (m/s);
u_s = bubble slip velocity (m/s);
W = width of the bubble core defined in Fig. 1 (cm);
x = horizontal distance from the nozzle exit defined in Fig. 1 (cm);
x_b = horizontal position of the bubble plume centerline (cm);
x_w = horizontal position of the water jet centerline (cm);
z = vertical distance from the nozzle exit defined in Fig. 1 (cm);
z_b = vertical position of the bubble plume centerline (cm);
z_w = vertical position of the water jet centerline (cm);
α = air concentration or local void fraction (%); and
ϵ = gas volume fraction at the nozzle defined by Eq. (2).

References

Amberg, H. R., Wise, D. W., and Aspitarte, T. R. (1969). "Aeration of streams with air and molecular oxygen." *Tappi J.*, 52(10), 1866–1871.

Boes, R. M., and Hager, W. H. (2003). "Two-phase flow characteristics of stepped spillways." *J. Hydraul. Eng.*, 129(9), 661–670.

Bombardelli, F. A., Buscaglia, G. C., Rehmann, C. R., Rincón, L. E., and García, M. H. (2007). "Modeling and scaling of aeration bubble plumes: A two-phase flow analysis." *J. Hydraul. Res.*, 45(5), 617–630.

Chanson, H. (2002). "Air-water flow measurements with intrusive, phase-detection probes: Can we improve their interpretation?" *J. Hydraul. Eng.*, 128(3), 252–255.

Clift, R., Grace, J. R., and Weber, M. E. (1978). *Bubbles, drops and particles*, Academic, New York.

Fast, A. W., and Lorenzen, M. W. (1976). "Synoptic survey of hypolimnetic aeration." *J. Envir. Engrg. Div.*, 102(6), 1161–1173.

Fonade, C., Doubrovine, N., Maranges, C., and Morchain, J. (2001). "Influence of a transverse flowrate on the oxygen transfer performance in heterogeneous aeration: Case of hydro-ejectors." *Water Res.*, 35(14), 3429–3435.

García, C. M., and García, M. H. (2006). "Characterization of flow turbulence in large-scale bubble-plume experiments." *Exp. Fluids*, 41(1), 91–101.

Iguchi, M., Okita, K., Nakatani, T., and Kasai, N. (1997). "Structure of turbulent round bubbling jet generated by premixed gas and liquid injection." *Int. J. Multiphase Flow*, 23(2), 249–262.

Jirka, G. H. (2004). "Integral model for turbulent buoyant jets in unbounded stratified flows. I: Single round jet." *Environmental Fluid Mechanics*, 4(1), 1–56.

Leitch, A. M., and Baines, W. D. (1989). "Liquid volume flux in a weak bubble plume." *J. Fluid Mech.*, 205, 77–98.

Lima Neto, I. E., Zhu, D. Z., and Rajaratnam, N. (2008a). "Air injection in water with different nozzles." *J. Environ. Eng.*, 134(4), 283–294.

Lima Neto, I. E., Zhu, D. Z., and Rajaratnam, N. (2008b). "Effect of tank size and geometry on the flow induced by circular bubble plumes and water jets." *J. Hydraul. Eng.*, 134(6), 833–842.

Lima Neto, I. E., Zhu, D. Z., and Rajaratnam, N. (2008c). "Bubbly jets in stagnant water." *Int. J. Multiphase Flow*, in press.

Lima Neto, I. E., Zhu, D. Z., Rajaratnam, N., Yu, T., Spafford, M., and McEachern, P. (2007). "Dissolved oxygen downstream of an effluent outfall in an ice-covered river: Natural and artificial aeration." *J. Environ. Eng.*, 133(11), 1051–1060.

McGinnis, D. F., and Little, J. C. (2002). "Predicting diffused-bubble oxygen transfer rate using the discrete-bubble model." *Water Res.*, 36(18), 4627–4635.

Milgram, H. (1983). "Mean flow in round bubble plumes." *J. Fluid Mech.*, 133, 345–376.

Morchain, J., Moranges, C., and Fonade, C. (2000). "CFD modelling of a two-phase jet aerator under influence of a crossflow." *Water Res.*, 34(13), 3460–3472.

Mueller, J. A., Boyle, W. C., and Pöpel, H. J. (2002). *Aeration: Principles and practice*, CRC, New York.

Murzyn, F., Mouaze, D., and Chaplin, J. R. (2005). "Optical fibre probe measurements of bubbly flow in hydraulic jumps." *Int. J. Multiphase Flow*, 31(1), 141–154.

Rainer, B., Fonade, C., and Moser, A. (1995). "Hydrodynamics of a new type of ejector." *Bioprocess Eng.*, 13(2), 97–103.

Rensen, J., and Roig, V. (2001). "Experimental study of the unsteady structure of a confined bubble plume." *Int. J. Multiphase Flow*, 27(8), 1431–1449.

Riess, I. R., and Fanneløp, T. K. (1998). "Recirculation flow generated by line-source bubble plumes." *J. Environ. Eng.*, 124(9), 932–940.

Ruzicka, M. C. (2000). "On bubbles rising in line." *Int. J. Multiphase Flow*, 26(7), 1141–1181.

Schierholz, E. L., Gulliver, J. S., Wilhelms, S. C., and Henneman, H. E. (2006). "Gas transfer from air diffusers." *Water Res.*, 40(5), 1018–1026.

Socolofsky, S. A., and Adams, E. E. (2002). "Multi-phase plumes in uniform and stratified crossflow." *J. Hydraul. Res.*, 40(6), 661–672.

SonTek. (1997). *Acoustic doppler velocimeter, technical documentation version 4.0*, San Diego.

Sun, T. Y., and Faeth, G. M. (1986a). "Structure of turbulent bubbly jets. I: Methods and centerline properties." *Int. J. Multiphase Flow*, 12(1), 99–114.

Sun, T. Y., and Faeth, G. M. (1986b). "Structure of turbulent bubbly jets. II: Phase property profiles." *Int. J. Multiphase Flow*, 12(1), 115–126.

Varley, J. (1995). "Submerged gas-liquid jets: Bubble size prediction." *Chem. Eng. Sci.*, 50(5), 901–905.

Water Pollution Control Federation (WPCF). (1988). *Aeration—Manual of practice—No. FD-13*, Alexandria, Va.

Whipple, W. J., and Yu, S. L. (1970). "Instream aerators for polluted rivers." *J. Sanit. Engrg. Div.*, 96(5), 1153–1165.

Wüest, A., Brooks, N. H., and Imboden, D. M. (1992). "Bubble plume modeling for lake restoration." *Water Resour. Res.*, 28(12), 3235–3250.

J. Hydraul. Eng., 2008, 134(12): 1722-1731